Computation of Temperature Elevation in Rabbit Eye Irradiated by 2.45-GHz Microwaves with Different Field Configurations

Akimasa Hirata[1], Soichi Watanabe[2], Masao Taki[3], Osamu Fujiwara[1], Masami Kojima[4,5], Kazuyuki Sasaki[5]

1: Department of Computer Science and Engineering, Nagoya Institute of Technology, Japan
2: National Institute of Information and Communications Technology, Tokyo, Japan
3: Department of Electrical Engineering, Tokyo Metropolitan University, Tokyo, Japan
4: Department of Ophthalmology, Kanazawa Medical University, Kanazawa, Japan
5: Division of Vision Research for Environmental Health, Medical Research Institute, Kanazawa Medical University, Japan

Correspondence to Akimasa Hirata (E-mail: ahirata@nitech.ac.jp)
Submitted to Health Phys. (PAPER)

Abstract

This study calculated the temperature elevation in the rabbit eye caused by 2.45-GHz near-field exposure systems. First, we calculated specific absorption rate distributions in the eye for different antennas, and then compared them with those observed in previous studies. Next, we re-examined the temperature elevation in the rabbit eye due to a horizontally-polarized dipole antenna with a C-shaped director, which was used in a previous study. For our computational results, we found that decisive factors of the SAR distribution in the rabbit eye were the polarization of the EM wave and antenna aperture. Next, we quantified the eye average SAR as 67 W/kg for the dipole antenna with an input power density at the eye surface of 150 mW/cm^2, which was specified in the previous work as the minimum cataractogenic power density. The effect of administrating anesthesia on the temperature elevation was 30% or so in the above case. Additionally, the position where maximum temperature in the lens appears is discussed due to different 2.45-GHz microwave systems. That position was found to appear around the posterior of the lens regardless of the exposure condition, which indicates that the original temperature distribution in the eye was the dominant factor.

Keywords—microwave-induced cataract, temperature elevation, bioheat equation, SAR (specific absorption rate)

1. Introduction

In accordance with the rapid spread of wireless communication systems, there has been increasing concern about adverse health effects due to microwave (MW) energy. For MW near-field exposures, safety standards/guidelines limit the peak spatial-average specific absorption rate (SAR) (ICNIRP 1998, IEEE C95.1 2005). In the ICNIRP guidelines (1998), the averaging mass is 10 g and the limit is 2.0 W/kg for public exposure. The background of this prescript is to prevent thermal damage in sensitive tissues from excess temperature elevation during partial-body MW exposure.

Substantial attention has been paid to eye tissues, since it has been reported that MW energy causes a variety of ocular abnormalities, including cataracts, due to high-intensity exposure (Elder 2003). Kramar et al. (1975) discussed MW-induced cataractogenic mechanisms using hypothermic rabbits. They concluded that temperature elevation is essential to produce a cataractogenic effect. Another work by the same group is referenced in the ICNIRP guidelines as one of the key papers. Guy et al. (1975) investigated the effects of MW energy on the lens of New Zealand White rabbits under systemic anesthesia. The minimum power density for cataract was determined to be 150 mW/cm^2 for duration of 100 min. Note that the threshold power density of MW depends on the time duration. In the above MW exposure, the peak local (or point) SAR was experimentally specified as 138 W/kg. However, that work did not quantify eye average SAR or peak spatial-average SAR, which is used as a measure for human protection in current guidelines/standards (ICNIRP 1998, IEEE C95.1 2005). These studies triggered many researchers to further investigate MW-induced cataracts (e.g., Guy et al. 1975; Kramar et al. 1975, 1978, Carpenter 1979, McAfee et al 1983, Barber 1990, Kamimura et al. 1994). In such works, different types of exposure systems, species, and conditions were adopted by different groups, complicating this research field. It is worth pointing out that rabbits were anesthetized in Guy et al. (1975) and Kramar et al. (1975). Our group paid attention to this point, and then measured temperature elevations in rabbit eyes with and without systemic anesthesia for MW near-field exposure (Kojima et al. 2004). Note that in the latter case local anesthesia was administered on the eye only. A major finding was that much higher temperatures were observed in the eyes of anesthetized than in those of unanesthetized rabbits. In order to give some insight into this problem, we developed a thermal computation model for rabbits (Hirata et al. 2006). Computational results in comparison with measurement then suggested that the thermoregulatory response of the anesthetized rabbit would be inactivated, together with reductions in blood perfusion and basal metabolism.

This study computationally investigated the temperature distribution in the rabbit eye due to MW irradiated from different 2.45-GHz MW exposure systems under the condition with and without anesthesia. Our thermal computation model for rabbits (Hirata et al. 2006) was used in

this analysis. Much attention was paid to the difference in SAR and temperature elevation due to different exposure antennas in the previous works. Particularly, this study quantified the eye average SAR due to an exposure system used in Guy et al. (1975), in order to bridge current guidelines (ICNIRP 1998) and the findings in that work (Guy et al. 1975). In addition, this study discussed the position where maximum temperature in the lens appears due to 2.45GHz-MW exposure systems.

2. Computational Model and Methods

2.1 Rabbit Phantom

An anatomically-based rabbit phantom with a resolution of 1 mm was considered in this study. This phantom was constructed on the basis of X-ray CT images for male pigmented rabbits (Dutch, 2.5 kg), which were taken at Kanazawa Medical University, Japan (Wake et al. 2002). The dimension of the phantom is 154 (W) X 325 (D) X 190 (H) cells. It is noteworthy that the thicknesses of most eye tissues, such as retina, choroid, and so forth are smaller than the spatial resolution of the phantom. Thus, the retina, choroid, and sclera were considered as a compound tissue, and their average electrical and thermal constants were used in our calculation. Similarly, the iris and ciliary body were treated as a compound tissue. The developed model is comprised of 12 tissues: skin, muscle, bone, fat, brain, CSF, anterior chamber, vitreous cavity, retina/choroid/sclera, iris/ciliary body, lens, and cornea. Retina/choroid/sclera was further classified into two based on the blood perfusion rate (Hirata et al. 2006). The eye model with a coordinate system is given in Fig. 1. The mass of the left eye, on which MW was irradiated, is 3.1 g.

2.2 Computational Method

The FDTD (Finite-Difference Time-Domain) method (Taflove and Hagness 2005) was used for investigating MW energy absorbed in the rabbit phantom. For the truncation of computational region, we adopted 12-layered perfectly matched layers as the absorbing boundary. In order to incorporate the rabbit phantom into the FDTD scheme, the electric constants of tissues are required. They are determined with the aid of the 4-Cole-Cole extrapolation (Gabriel 1996).

Temperature variation in the rabbit phantom was followed in the time domain by solving the bio-heat equation (Pennes 1948). The SAR obtained by the FDTD method is substituted into the bio-heat equation as the heat source. Let us give some review of our thermal computation model. A generalized bioheat equation is given by the following equation:

$$C(\boldsymbol{r})\rho(\boldsymbol{r})\frac{\partial T(\boldsymbol{r},t)}{\partial t} = \nabla\cdot(K(\boldsymbol{r})\nabla T(\boldsymbol{r},t)) + \rho(\boldsymbol{r})SAR(\boldsymbol{r}) + A(\boldsymbol{r},t) - B(\boldsymbol{r},T(\boldsymbol{r},t))(T(\boldsymbol{r},t) - T_B(\boldsymbol{r},t)) \quad (1)$$

where $T(\boldsymbol{r},t)$ and $T_B(\boldsymbol{r},t)$ denote the temperatures of tissue and blood, respectively, where $\boldsymbol{r}$ and t are the position vector and the time. C represents the specific heat of tissue, K the thermal conductivity of tissue, A the basal metabolism per unit volume, and B the term associated with blood perfusion. The thermal parameters of rabbit tissues were estimated on the basis of their water content, together with a comparison between computed and measured temperatures (Hirata et al. 2006). When neglecting the sweating effect (Marai et al. 2002), the boundary condition between air and tissue for Eq. (1) is given by the following equation:

$$-K(\boldsymbol{r})\frac{\partial T(\boldsymbol{r},t)}{\partial n} = H\cdot(T_s(\boldsymbol{r},t) - T_e(t)) \quad (2)$$

where H, T_s, and T_e denote, respectively, the heat transfer coefficient including the effect of radiative and convective heat loss, body surface temperature, and air temperature. For taking into account body-core temperature elevation in the bioheat equation, it is reasonable to consider the blood temperature as a variable of time $T_B(\boldsymbol{r},t) = T_B(t)$: namely, the blood temperature is assumed to be spatially constant over the whole body, since the blood circulates throughout the human body in one minute or less (Follow and Neil 1971). Then, the blood temperature variation is given by the following equation (Bernardi et al. 2003):

$$T_B(t) = T_{B0} + \int_t \frac{Q_{BT}(t)}{C_B\rho_B V_B}dt \quad (3)$$

where T_{B0} and Q_{BT} are the blood temperature given at the initial state and the net rate of heat acquisition of blood from body tissues. C_B (=4000 J/kg·°C), ρ_B (=1050 kg/m^3), and V_B denote the specific heat, mass density, and total volume of blood, respectively. The effectiveness of this formula was confirmed by comparing with the measured rectal temperature elevation (Hirata et al. 2006). In the present study, the blood temperature T_{B0} is chosen as 39.3°C, which is average rectal temperature of the pigmented rabbit (Dutch) (Experimental Data Book 1998). Our formula for thermoregulatory response is mainly based on the works by Spiegel (1984), Hoque and Gandhi (1988), and Bernardi et al. (2003). These studies paid attention to the thermoregulatory response of humans. For this reason, we have verified the applicability of such computation models to rabbits through a parametric study (Hirata et al. 2006).

In the case without anesthesia, the dependency of blood perfusion rate on tissue temperature was considered as thermoregulatory response: namely the term associated with the blood perfusion rate was treated as the function of temperature elevation. In the case with systemic anesthesia, on the other hand, the thermoregulation is equated with inactivation. Then, the blood perfusion rate and basal metabolism were reduced by 20% over the whole body (Hirata et al.

2006). Note that anesthetic depth depends on individuals and body parts (Tuma et al. 1981), and thus the computational result with above reduction ratio would include some uncertainty. Our computational results, however, would give insight on standard behavior of rabbit temperature elevation due to MW energy, since representative measured data were used to determine thermal parameters of tissues, excluding the outlying value from more than ten sample data (Hirata et al. 2006). Additional point to be stressed here is that our modeling is that unlike previous works that focused on eye temperature elevations (Emery et al. 1975; Lagendjik 1982; Hirata et al. 2000), this computation model takes into account the whole body model, and then body-core temperature (blood temperature) is changed with time.

2.3. Wave Sources

As wave sources, we considered a dielectric-filled waveguide antenna (Wake et al. 2002), a dipole antenna with a C-shaped reflector (Guy et al. 1974) which was used in Guy et al. (1975), and a plane wave. The horizontal (H) and vertical (V) polarizations were considered. Note that we define the horizontal and vertical polarizations as defined in Fig. 2. The frequency considered in this study is limited to 2.45 GHz since most previous studies investigated microwave-induced cataract at this frequency (Guy et al 1975; Carpenter 1979; Kamimura et al 1994, e.g.). In our computation, MW was incident perpendicular to the eye surface. Fig. 2 illustrates (a) a dipole antenna with a C-shaped reflector and (b) a waveguide antenna. The distances *d* were 50 mm (Guy et al. 1975) and 30 mm (Wake et al. 2002), respectively. At these antenna-eye separations, the input impedance of the dipole antenna with the C-shaped reflector was changed due to the presence of the rabbit. Taking into account the reflection due to the rabbit, the power density at the eye surface was compensated. On the other hand, such degradation of antenna output power was marginally observed in the latter antenna. In the following discussion, the power density of MW is defined at the eye surface for the near-field exposure systems.

3. Computational Results

3.1. Effect of Wave Sources on Eye SAR

Figs. 3 (a) and (b) show the one-dimensional SAR distributions in the eye along the x-axis for the vertical and horizontal polarizations, respectively. Incident power density at the eye surface is 1.0 mW/cm^2. The origin of the coordinate system was on the eye surface. Measured results in Guy et al. (1975) are also plotted for comparison. Note that New Zealand White rabbits were used in Guy et al. (1975), while pigmented rabbits (Dutch) were considered in the present study. The body weight of the former (4 kg) is larger than that of the latter (2.5 kg), while there is no clear difference in the eye diameter. As is evident from these figures, one of the dominant

factors determining the SAR distribution is the polarization of EM waves, although the eyeball is almost a sphere. It is known that the polarization effect on SAR in humans becomes obvious when the dimensions of body, body parts, or organs are comparable to the wavelength (Gandhi 1980; Hirata et al. 2000), which is attributed to a standing wave. The whole body resonates electrically when the body dimension and the wavelength in free space are comparable (Gandhi 1980). In the case of the human eye (Hirata et al. 2000), a standing-wave in the eye was formed around 2 GHz and the EM power absorption was dependent on the polarization and frequency of the incident wave. Note that the eye diameter of the human is 24 mm, while that of the rabbit is 17 mm. Thus, a standing wave in the eye could happen in case of rabbits at the frequency of 2.45 GHz. The SAR in the lens and vitreous cavity for the horizontal polarization was largest for the plane wave, then for the dipole antenna with the reflector, followed by the waveguide antenna. The reason for this discrepancy is the diffraction of EM waves. The aperture of the dipole antenna with the reflector is larger than the waveguide antenna, as indicated in Fig. 2: namely, the antenna aperture is a dominant factor for the SAR amplitude. The same tendency was observed for SARs due to exposures with the vertical polarization. Note that this study does not discuss the effect of frequency on the SAR distribution. The frequency is another dominant factor which affects the SAR distribution: see computational dosimetry for human eye in Hirata *et al* (2000), Flyckt *et al* (2007), Wainwright (2007).

The ratio of eye average SAR to whole-body average SAR is investigated for different exposure systems with the vertical or horizontal polarizations. This index would be one of the most important factors when discussing the localized MW exposure. The whole-body SAR is close related to temperature elevation despite different SAR distribution (Hirata et al 2007). In other words, this index suggests that the localized temperature elevation is realized without whole-body temperature elevation. It is worth noting that the whole-body temperature elevation may result in excessive thermal stress, resulting in death before microwave-induced cataract, as Appleton et al. (1975) has shown for far-field exposure. On the other hand, even for localized exposure with the dipole antenna with C-shaped director (Guy et al. 1975), the rectal temperature elevation was observed. This would be because the total EM energy absorbed in rabbit bodies could not be neglected even for intense localized exposure (see Yamaguchi et al. 2003 for rats, e.g.), which is attributed to a small dimension of rabbit body as compared with the wavelength of MW. For the localized exposure to the eye with the waveguide antenna at the power density of 300mW/cm^2, the eye-average SAR and the whole-body average SAR were 92.2 W/kg and 1.29 W/kg, respectively. Based on such a calculation, the ratio of eye average SAR to whole-body average SAR were calculated for different experimental systems and then listed in Table 1. From this table, the ratio of eye average SAR to whole-body SAR was found to be not easily predictable, since the polarization and antenna aperture affect both eye and body

SAR.

Verification of Thermal Modeling in Comparison with Previous Studies

Hirata et al.. [2006] developed a thermal computation model for rabbits in comparison with computed and measured temperature elevations. For further verifying the effectiveness of our thermal model, we compared with the result in Guy et al. (1975). We chose the case for the incident power density of 150 mW/cm^2 for the duration of 100 min. In our calculation, anesthetized and unanesthetized rabbits were considered. In our modeling for the anesthetized rabbit, thermoregulatory response was ignored and metabolic rate was reduced by 20 % on the basis of our measurements (Kojima et al. 2004; Hirata et al. 2006). It is worth noting that a highly simplified heat transfer model was used in Guy et al. (1975): the eye was assumed to be thermally isolated from the body (Emery et al. 1975; Lagendjik 1982), and the effect of anesthesia on blood perfusion was not taken into account. On the other hand, heat transfer coefficient was determined in comparison with the measurement. The computational error due to this simplification is given in Hirata (2007). As seen from Fig. 4, the steady-state temperature without MW exposure is in excellent agreement with that in Schwartz and Feller (1962). The computed temperature after 100 min. passed with MW energy is in good agreement with that in Guy et al. (1975). One of the main reasons for this small difference between the eye temperatures would be caused by the difference in the body-core temperature elevation. This difference in the body-core temperature would be caused by the difference in the body weight between pigmented rabbits and New Zealand White rabbits. For localized exposure to the eye, the total EM energy absorbed in rabbits does not differ so much even for different body weight. On the other hand, more energy is required for a rabbit with larger weight, i.e., larger blood volume, to elevate the blood temperature (see Eq. (3)).

Fig. 4 also suggests again that the temperature elevation is overestimated due to the administration of anesthesia, just as in Hirata et al. (2006). The temperature elevation in the lens was in the range of 2.6-7.8 ^{o}C with anesthesia, while 1.9-5.4 ^{o}C without anesthesia; namlely, overestimation of temperature elevation when neglecting the thermoregulatory response was 30% or so in our computational model. Note that this magnitude of the overestimation would depend on the anesthetic depth of individual rabbit, while it is out of the scope in the present study to discuss the difference of temperature elevation caused by the individual anesthetic depth. Since we used the numeric rabbit model based on Dutch, the body weight (2.5 kg) is smaller than that in Guy et al (1975) of 4 kg. The whole-body SAR in Dutch would be larger than that for the weight of 4 kg by 40% due to the difference in the weight. This rough estimation would be reasonable since EM power is absorbed around the eye for localized exposure. Note that the whole-body average SAR is a good measure for correlating the

body-core or blood temperature elevation (Hirata et al, 2007). Now the body-core temperature or blood temperature elevation was 1.3 ^{o}C in this computational scenario, the body-core temperature elevation in 4.0 kg rabbit would be 0.5 ^{o}C smaller than that in our calculation. This difference in the body-core temperature would influence local temperature. Taking into account this compensation, better agreement with Guy et al (1975) would be obtained.

3. 2. Temperature Elevation in Rabbit Eye Due to Localized Exposure Systems

Fig. 5 shows the temperature elevation at the center of the lens for different EM power densities at the eye surface. As a wave source, the waveguide antenna with the vertical polarization is used. As seen from this figure, the temperature elevates rapidly in the first 10 minutes, and then keeps elevating gradually with time. This result coincides with the results in Guy et al. (1975). Fig. 6 shows the time evolution of blood temperature elevation due to the waveguide antenna with the vertical polarization for different power densities. As seen from this figure, the blood temperature elevates almost linearly with the time and power densities. The reason why the body-core temperature keeps elevating is that the sweating effect in rabbits can be neglected (Marai et al 2002).

Next, the position where the maximum temperature appears in the lens is investigated due to different exposure system. The threshold temperature in the lens which induces cataract is said to be 41-43 ^{o}C (Guy *et* al. 1975; Elder 2003). Fig. 7 shows the temperature distribution in the eye after 60 min. passed with MW energy. The vertical polarization is chosen in this discussion. The power density of MW at the eye surface is determined so that the maximum temperature in the lens becomes 42 ^{o}C; 240 mW/cm^2 for the waveguide antenna, 140 mW/cm^2 for the dipole antenna with the reflector, and 34 mW/cm^2 for the plane wave, respectively. As seen from this figure, the maximum temperature in the lens appears around its posterior for all three cases. These positions coincide with the result in Guy et al. (1975), although the polarization and/or exposure systems are different.

4. Discussion

Guy et al. (1975) specified the threshold power density of MW-induced cataract formation as 150 mW/cm^2 for duration of 100 minutes. At that time, the peak point SAR was estimated as 138 W/kg. The peak voxel SAR on the center line was 143 W/kg in our calculation, and was in good agreement with that in the previous study. Note that peak voxel SAR in the whole eye of our calculation was 168 W/kg. Using our 2.5 kg Dutch rabbit model, we estimated that the eye SAR is 67 W/kg in the 4 kg white albino rabbits used in the Guy et al. (1975) study. Note that the averaging mass does not coincide with that in the current guideline (ICNIRP 1998), as the mass of the rabbit eye is 3.1 g.

In Guy et al. (1975), a cataract was formed in the posterior of the lens, and that position coincides with that of maximum temperature due to 2.45 GHz microwave energy, as shown in Fig. 7. Let us discuss further the generality of this position for different sources.

First, the waveguide antenna with the vertical polarization is chosen to investigate the effect of incident power density. As the input power density, 100, 200, 300, and 400 mW/cm^2 were considered. The duration of exposure was 60 min. Fig. 8 shows the temperature elevation distribution in the eye normalized by the maximum temperature elevation at each incident EM power density. The maximum temperature elevations for these power densities were 2.4, 4.3, 5.9, and 7.5 ^{o}C, suggesting the nonlinearity of temperature elevation due to thermoregulatory response. From Fig. 8, the normalized temperature elevations in the eye were marginally affected by the input power density despite of the physiological response and body-core temperature elevation. The difference of up to 5% was observed in the retina/choroid/sclera and fat/muscle, while smaller in the remaining eye part. This insensitivity of temperature elevation distribution in the eye to the incident power density would be caused by the nonexistence of blood perfusion in the humor and the lens. The thermoregulatory response considered in our modeling is the temperature-dependent blood perfusion rate only, and thus does not affect the temperature distribution in the eye so much. The above discussion implies that the temperature distribution in the eye with MW energy is roughly estimated from the initial temperature distribution and the temperature elevation due to MW energy for arbitrary power density.

Next, the temperature elevation due to MW energy is shown in Fig. 9 for different sources with eye-average SAR of 1.0 W/kg. As seen from this figure, the temperature elevation distribution depends on each exposure system. For the dipole antenna with the reflector, the maximum temperature elevation appears around the posterior of the eye. The maximum temperature due to MW energy never fails to appear around the posterior part of the eye, since the maximum temperature in the lens at the initial state is at the posterior of the lens. For the remaining sources, the maximum temperature elevation appears anterior or center part of the lens. However, the temperature elevation distribution in the lens is rather uniform. The threshold temperature in the lens which induces cataract is said to be 41-43 ^{o}C (Guy et al. 1975; Elder 2003). It is sufficient to consider temperature elevations of less than 7 ^{o}C since the thermally-steady state temperature is 34 ^{o}C at the front of the lens and 36 ^{o}C at the back of the lens, as seen from Fig. 4. For the temperature elevation less than 7°C, the effect of initial temperature distribution could be a more dominant factor than the temperature elevation due to MW energy. Although not shown here for avoiding repetition, the same tendency was observed for the horizontal polarization. From these results, maximum temperature elevation in the lens would appear around its posterior for different near-field and far-field exposure systems at 2.45 GHz.

5. SUMMARY

This study investigated temperature elevation in the rabbit eye due to 2.45-GHz near-field exposure systems. Peak spatial-average SAR is used as a measure for human protection from RF near-field exposures in safety guidelines (ICNIRP 1998), although its rationale is unclear. One of the representative works was conducted by Guy et al. (1975), in which a minimal power density for MW-induced cataract was specified. That work did not quantify peak spatial-average SAR, which is used as a metric in current guidelines. In order to re-investigate this problem, we used our thermal computation model (Hirata et al. 2006), which takes into account the whole rabbit phantom and the blood temperature variation.

First, we calculated the SAR distributions for different antennas and compared them with those in previous papers, and found that dominant factors determining the SAR distribution in the eye are the polarization of the EM wave and antenna aperture at 2.45 GHz. For the dipole antenna with the C-shaped reflector used in Guy et al. (1975), eye averaged SAR in Guy et al. (1975) was estimated as 67 W/kg.

Next, we re-examined temperature elevation in the rabbit eye due to the horizontally-polarized dipole antenna with the reflector. Our computed temperature distribution was in good agreement with that in Guy et al. (1975). The effect of administrating anesthesia on temperature elevation was also estimated, since anesthesia was applied in Guy et al. (1975). The computational results suggested that the administration of the anesthesia causes the overestimation of temperature elevation in the lens by 30% or so.

Furthermore, we discussed the position where a maximum temperature in the lens appears for 2.45-GHz microwave energy, since it appears around the posterior in the Guy's work. That that position was found to appear around its posterior for all exposure systems considered in this study including near-field and far-field sources. The dominant factor was caused by the steady-state temperature without MW exposure.

In Kramar et al. (1978), cataracts were formed in rabbit eyes, while not in monkey eyes. The authors in that study attributed this difference to different structure around the eye. In future work, we will examine the temperature elevation in the human eye by extrapolating our developed thermal model for rabbits to humans.

ACKNOWLEDGEMENTS

The authors would like to thank Prof. Y. Kamimura (Utsunomiya University, Japan) and Dr. K. Wake (NICT, Japan) for their useful advice in this work. This work was partially supported by International Communications Foundation, Japan.

References

Appleton B, Hirsch S, Kinion RO, Soles M, McCrossan GC, Neidlinger RM. Investigation of single exposure microwave ocular effects at 3000 MHz. Ann. NY. Acad. Sci. 247: 125-135; 1975

Barber BJ, Schaefer DJ, Gordon CJ, Zawieja DC, Hecker J. Thermal effects of MR imaging: Worst-case studies on sheep. Am J Roentgenol 155: 1105-1110; 1990.

Bernardi P, Cavagnaro M, Pisa S, Piuzzi E. Specific absorption rate and temperature elevation in a subject exposed in the far-field of radio-frequency sources operating in the 10-900-MHz range. IEEE Trans Biomed Eng 50: 295-304; 2003.

Carpenter RL. Ocular effects of microwave radiation. Bull NY Acad. Med.: 1048-1057; 1979.

Emery AF, Kramar P, Guy AW and Lin JC. Microwave induced temperature rises in rabbit eyes in cataract research J Heat Transfer 97: 123-28; 1975.

Elder J. Ocular effects of radiofrequency energy. Bioelectromagnetics Supplement 24: S148-61; 2003.

Experimental Data Book Japan SLC Inc 1998

Flyckt VMM, Raaymakers BW, Kroeze H, Lagendijk JJW. Calculation of SAR and temperature rise in a high-resolution vascularized model of the human eye and orbit when exposed to a dipole antenna at 900, 1500 and 1800 MHz Phys. Med. Biol: 52 2691-2701; 2007.

Follow B and Neil E Eds. Circulation. New York: Oxford Univ. Press; 1971.

Gabriel C. Compilation of the dielectric properties of body tissues at RF and microwave frequencies. Final Tech Rep Occupational and Environmental Health Directorate. AL/OE-TR-1996-0037 (Brooks Air Force Base, TX: RFR Division); 1996.

Gandhi OP. State of the knowledge for electromagnetic absorbed dose in man and animals. Proc IEEE 68: 24-32; 1980.

Guy AW, Lehmann JF, Stonebridge JB. Therapeutic applications of electromagnetic power. Proc

IEEE 62: 55-75; 1974.

Guy AW, Lin JC, Kramar PO, Emery A. Effect of 2450-MHz radiation on the rabbit eye. IEEE Trans Microwave Theory & Tech 23: 492-98; 1975.

Hirata A, Matsuyama S, Shiozawa T. Temperature rises in the human eye exposed to EM waves in the frequency range 0.6 - 6 GHz. IEEE Trans Electromagnetic Compt 42: 386-93; 2000.

Hirata A and Shiozawa T. Correlation of maximum temperature increase and peak SAR in the human head due to handset antennas. IEEE Trans Microwave Theory & Tech 51: 1834-41; 2003.

Hirata A. Temperature increase in human eyes due to near-field and far-field exposures at 900 MHz, 1.5 GHz, and 1.9 GHz. IEEE Trans Electromagnetic Compt 47: 68-76; 2005.

Hirata A, Watanabe S, Kojima M, Hata I, Wake K, Taki M, Sasaki K, Fujiwara O, Shiozawa T. Computational verification of anesthesia effect on temperature variation in rabbit eyes exposed to 2.45-GHz microwave energy. Bioelectromagentics 27: 602-612; 2006.

Hirata A. Improved heat transfer modeling of the eye for electromagnetic wave exposures. IEEE Trans Biomed Eng. in press; 2007a.

Hirata A, Asano T, Fujiwara O. Improved heat transfer modeling of the eye for electromagnetic wave exposures. IEEE Trans Biomed Eng. 54: 959-961; 2007.

Hoque M, Gandhi OP. Temperature distributions in the human leg for VLF-VHF exposures at the ANSI recommended safety levels. IEEE Trans Biomed Eng 35: 442-449; 1988.

International Commission on Non-Ionizing Radiation Protection (ICNIRP). Guidelines for limiting exposure to time-varying electric, magnetic and electromagnetic fields (up to 300 GHz). Health Phys 74: 494-522; 1998.

IEEE C95.1 IEEE Standard for Safety Levels with Respect to Human Exposure to Radio Frequency Electromagnetic Fields, 3 kHz to 300 GHz 2005.

Kamimura Y, Saito K, Saiga T, Amemiya Y. Effect of 2.45 GHz microwave irradiation on

monkey eyes. IEICE Trans Commun E77-B: 762-765; 1994.

Kojima M, Hata I, Wake K, Watanabe S, Yamanaka Y, Kamimura Y, Taki M and Sasaki K. Influence of anesthesia on ocular effects and temperature in rabbit eyes exposed to microwaves. Bioelectromagentics 25: 228-233; 2004.

Kotte A, vanLeeuwen G, deBree J, vanderKoijk J, Crezee H, Lagendijk J. A description of discrete vessel segments in thermal modeling of tissues. Phys Med Biol 41: 865-884; 1996.

Kramar PO, Emery AF, Guy AW, Lin JC. The ocular effects of microwaves on hypothermic rabbits: a study of microwave cataractogenic mechanisms. Annals of NY Academy of Sci 247: 155-165; 1975.

Kramar P, Harris C, Emery AF and Guy AW. Acute microwave irradiation and cataract formation in rabbits and monkeys. J. Microwave Pow. 13: 239-249; 1978.

Lagendijk JJ. A mathematical model to calculate temperature distributions in human and rabbit eyes during hyperthermic treatment. Phys Med Biol 27: 1301-1311; 1982.

Marai IFM, Habeeb AAM, Gad AE. Rabbit's productive, reproductive and physiological performance traits as affected by heat stress: a review. Livestock Prod Sci 78: 71-90; 2002.

McAfee RD, Oritiz-Lugo R, Bishop R, and Gordon R. Absence of deleterious effects of chronic microwave radiation on the eyes of Rhesus monkeys. Ophthalmology 90: 1243-1245; 1983.

Pennes HH. Analysis of tissue and arterial blood temperature in resting forearm. J Appl Physiol 1: 93-122; 1948.

Schwartz B, Feller MR. Temperature gradients in the rabbit eye Invest. Opth. 1: 513-521; 1962.

Spiegel RJ. A review of numerical models for predicting the energy deposition and resultant thermal responses. IEEE Trans Microwave Theory & Tech 32: 730-746; 1984.

Taflove A, Hagness S. Computational Electrodynamics: The Finite-Difference Time-Domain Method: 3rd Ed. Norwood. MA: Artech House; 2005.

Tell RA, Harlen F. A review of selected biological effects and dosimetric data useful for development of radiofrequency safety standards for human exposure. J Microwave Pow 14: 405-24; 1979.

Tuma RF, Irion GL, Vasthare US, Heinel LA. Age-related changes in regional blood flow in the rat. Am J Physiol 249: H485-H491; 1985.

Yamaguchi H, Tsurita G, Ueno S, Watanabe S, Wake K, Taki M, and Nagawa H. 1439 MHz pulsed TDMA fields affect performance of rats in a T-maze task only when body temperature is elevated. Bioelectromagnetics 24: 223-230; 2003.

Wainwright P. Computational modeling of temperature rises in the eye in the near field of radiofrequency sources at 380, 900 and 1800 MHz. Phys Med Biol 52: 3335-3368; 2007.

Wake K, Hongo H, Watanabe S, Yamanaka Y, Taki M, Kamimura Y, Uno T, Kojima M, Hata I, Sasaki K. Localized exposure system of 2.45 GHz microwave of the rabbit eye. Proc 27th URSI General Assembly; 2002: KAP6.

Table & Figure Captions

Tab. 1. Ratio of eye-average SAR to whole body average SAR for (i) plane wave, (ii) dipole antenna with C-shaped director, and (iii) waveguide antenna.

Fig. 1. Top view of rabbit model across the center of left eye with the coordinate system with the definition of x-axis.

Fig. 2. View of (a) dipole antenna with C-shaped reflector with horizontal polarization and (b) dielectric-filled waveguide antenna with vertical polarization.

Fig. 3. SAR distributions in rabbit eye for different sources: (a) horizontal and (b) vertical polarizations. Regions I, II, III, and IV correspond to cornea/ anterior chamber, lens, and vitreous cavity, fat/muscle layer, respectively.

Fig. 4. Temperature distribution in the eye with and without MW energy due to the dipole antenna with the reflector (100 min. 150mW/cm^2). In our computation, anesthetized and unanesthetized conditions are considered. Refer to Fig.3 for the definition of I, II, III, and IV.

Fig. 5. Time evolution of temperature at the center cell of lens for different power densities due to waveguide antenna with vertical polarization.

Fig. 6. Time evolution of blood temperature elevation due to waveguide antenna with the vertical polarization for different power densities.

Fig. 7. Temperature distribution in the eye due to different exposure systems (240 mW/cm^2 for the waveguide antenna, 140 mW/cm^2 for the dipole antenna with the reflector, and 34 mW/cm^2 for the plane wave). Refer to Fig.3 for the definition of I, II, III and IV.

Fig. 8. Temperature elevation in the eye normalized by maximum temperature rise in the eye for different EM power densities. Refer to Fig.3 for the definition of I, II, III and IV.

Fig. 9. Temperature elevation distribution in the eye at the thermally-steady state. The eye-average SAR was 1W/kg. Refer to Fig.3 for the definition of I, II, III and IV.

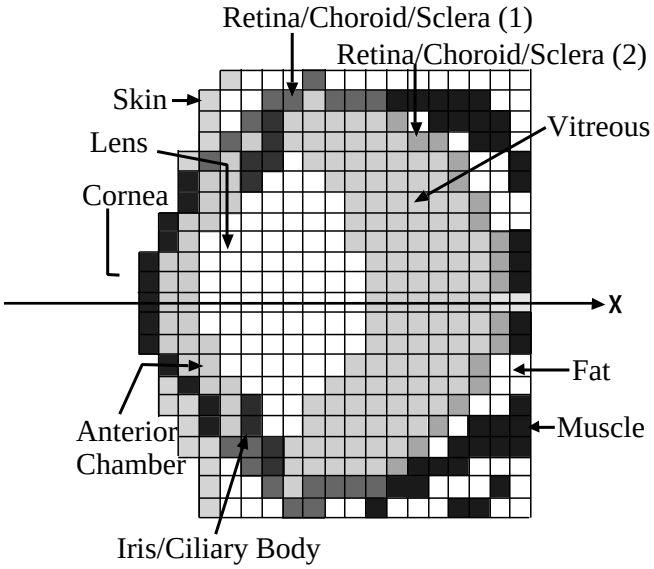
Retina/Choroid/Sclera (1)
Retina/Choroid/Sclera (2)
Skin
Vitreous
Lens
Cornea
X
Fat
Anterior
Chamber
Muscle
Iris/Ciliary Body

Fig. 1.

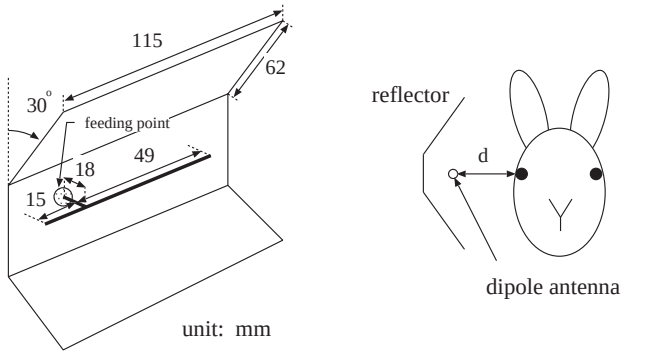
115
62
30°
feeding point
49
18
15
unit: mm
reflector
d
dipole antenna

(a)

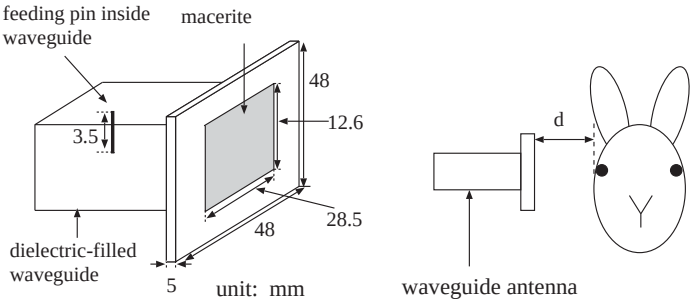
feeding pin inside
waveguide
macerite
48
12.6
3.5
28.5
48
dielectric-filled
waveguide
5
unit: mm
d
waveguide antenna

(b)

Fig. 2.

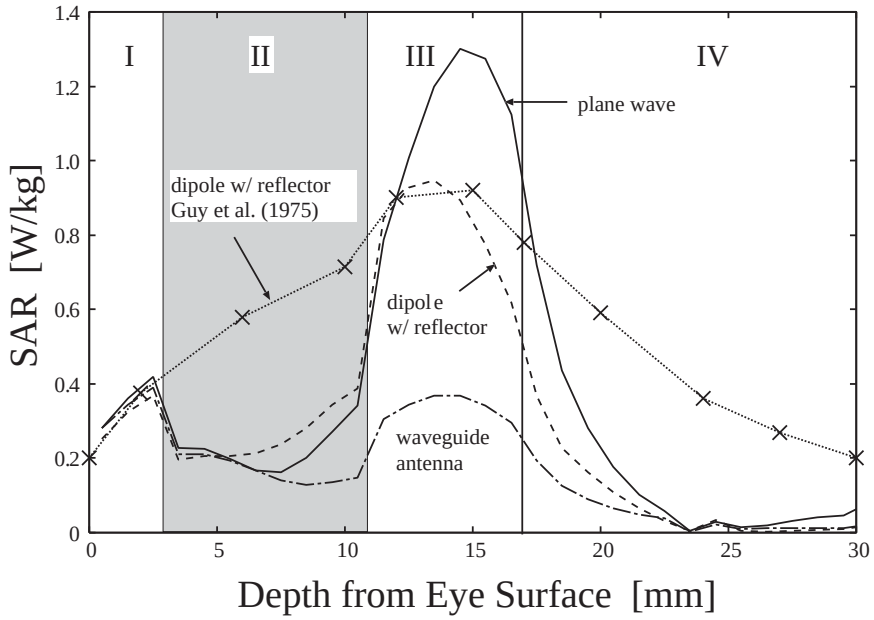
I
II
III
IV
plane wave
dipole w/ reflector
Guy et al. (1975)
dipole
w/ reflector
waveguide
antenna
SAR [W/kg]
Depth from Eye Surface [mm]

(a)

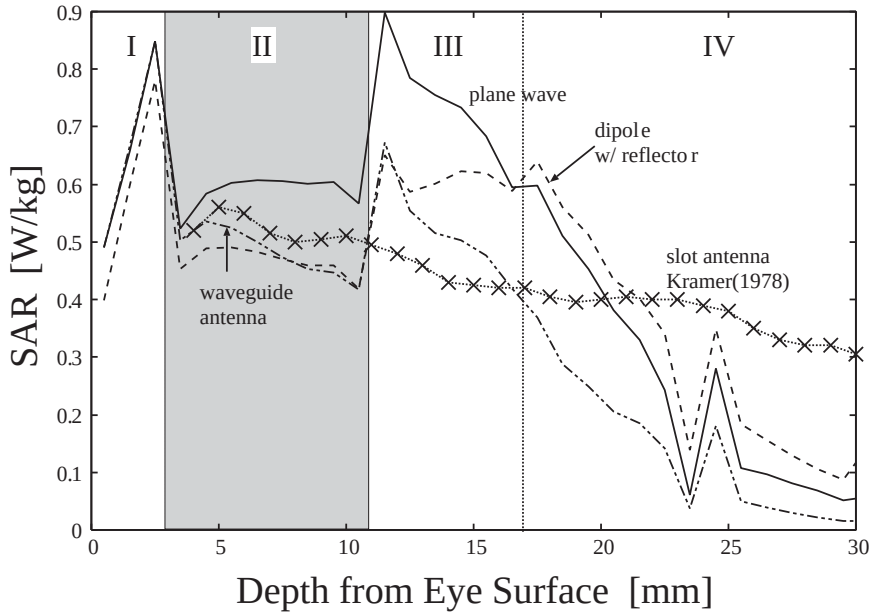
I
II
III
IV
plane wave
dipole
w/ reflector
slot antenna
Kramer(1978)
waveguide
antenna
SAR [W/kg]
Depth from Eye Surface [mm]

(b)

Fig. 3.

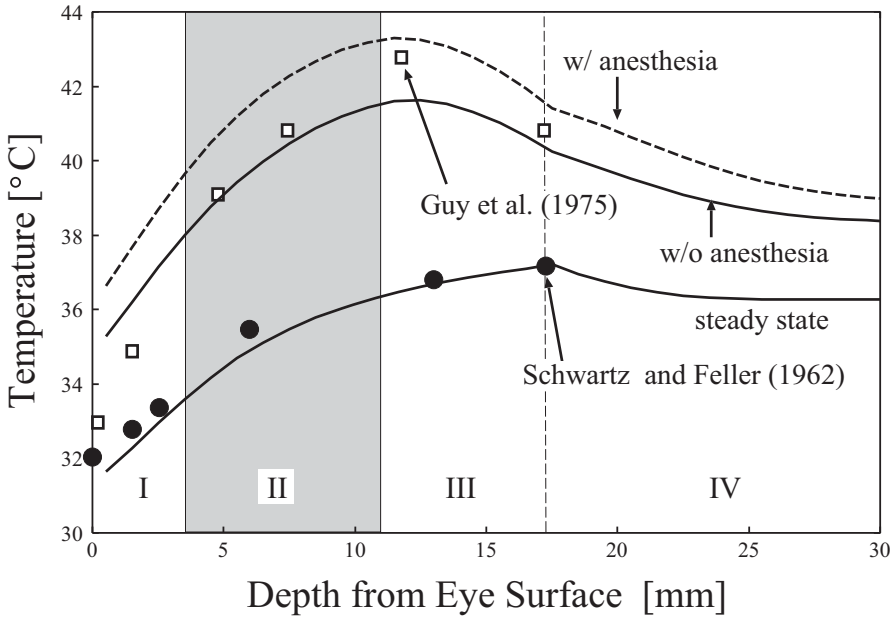
Temperature [°C]
Depth from Eye Surface [mm]
w/ anesthesia
Guy et al. (1975)
w/o anesthesia
steady state
Schwartz and Feller (1962)
I
II
III
IV

Fig. 4.

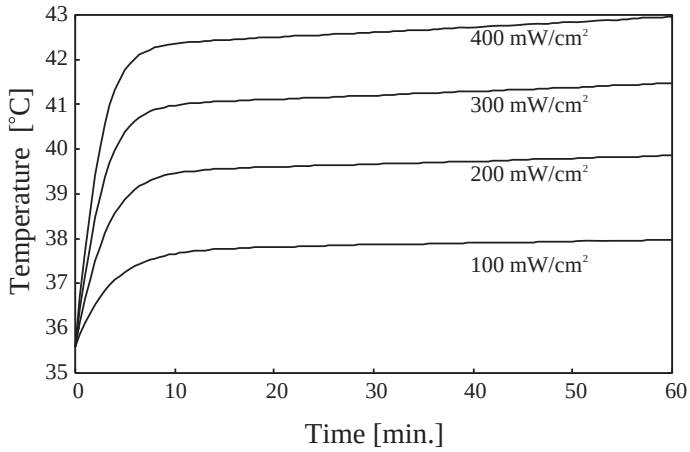
Temperature [°C]
Time [min.]
400 mW/cm²
300 mW/cm²
200 mW/cm²
100 mW/cm²

Fig. 5

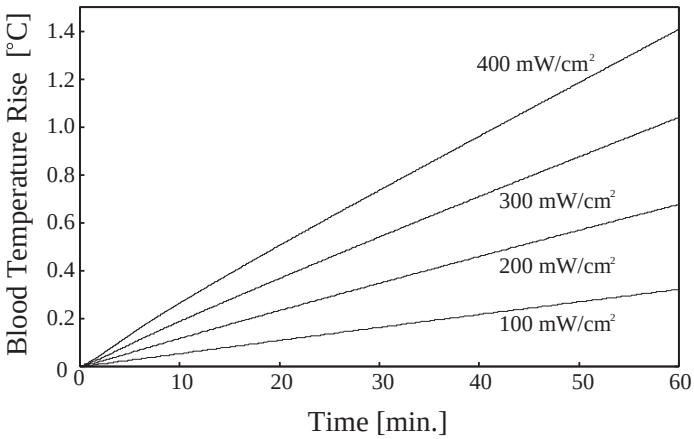
Blood Temperature Rise [°C]
1.4
1.2
1.0
0.8
0.6
0.4
0.2
0
0
10
20
30
40
50
60
Time [min.]
400 mW/cm²
300 mW/cm²
200 mW/cm²
100 mW/cm²

Fig. 6.

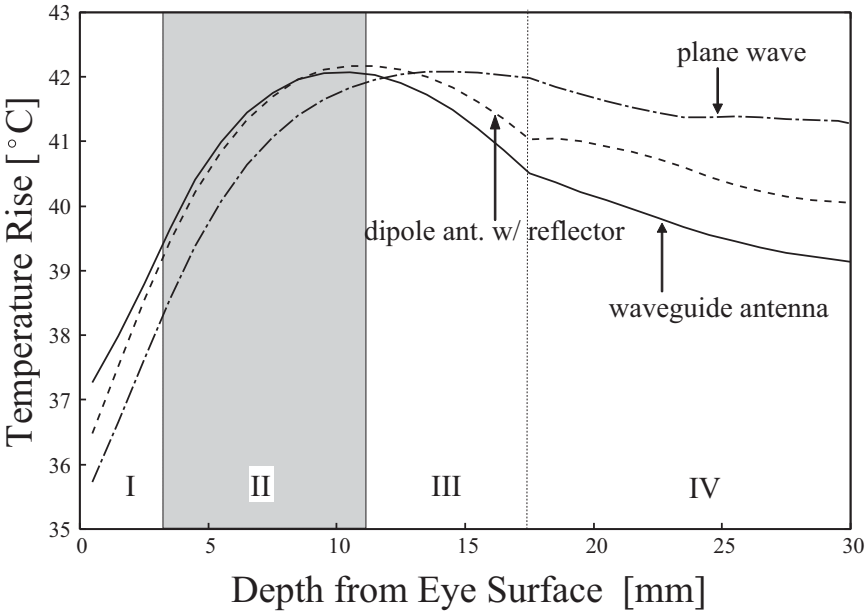
Temperature Rise [°C]
43
42
41
40
39
38
37
36
35
0
5
10
15
20
25
30
Depth from Eye Surface [mm]
plane wave
dipole ant. w/ reflector
waveguide antenna
I
II
III
IV

Fig. 7.

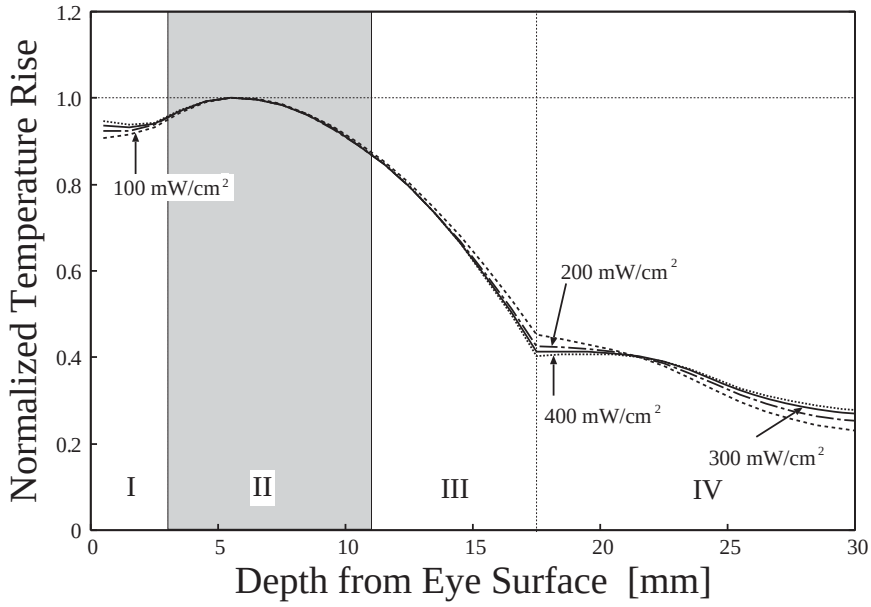
Normalized Temperature Rise
Depth from Eye Surface [mm]
100 mW/cm 2
200 mW/cm 2
400 mW/cm 2
300 mW/cm 2
I
II
III
IV

Fig. 8

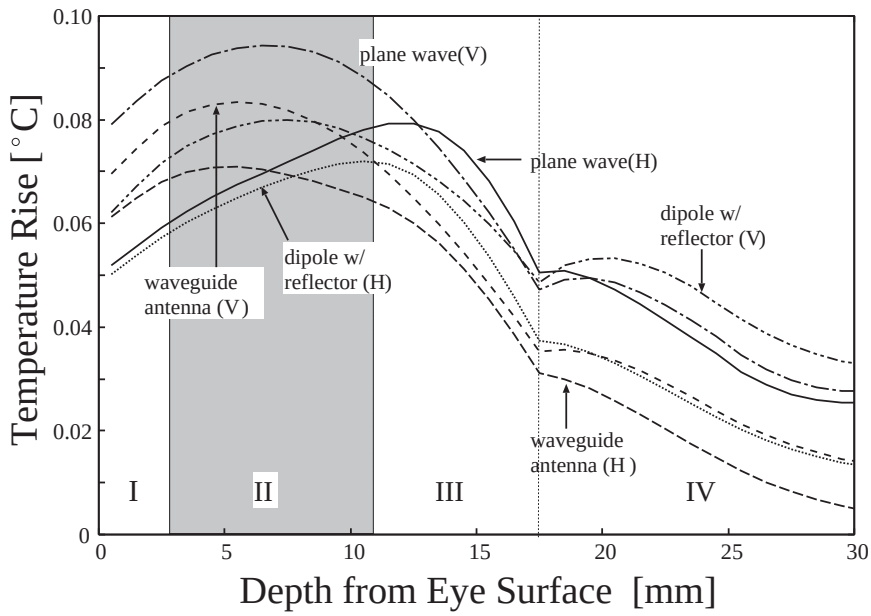
Temperature Rise [°C]
Depth from Eye Surface [mm]
plane wave(V)
plane wave(H)
dipole w/
reflector (V)
dipole w/
reflector (H)
waveguide
antenna (V)
waveguide
antenna (H)
I
II
III
IV

Fig. 9